Automatic Reference Color Selection for Adaptive Mathematical Morphology and Application in Image Segmentation

Huang-Chia Shih, *Member, IEEE*, and En-Rui Liu

***Abstract*— This paper proposes a novel automatic reference color selection (ARCS) scheme for the adaptive mathematical morphology (MM) method, and is specifically designed for color image segmentation applications. Because of the main advantages of being intuitive and simple, in the past decade, it has contributed to the growing popularity of binary and gray-scale MM processing. However, the MM process typically neglects the details of reference color determination. Applying other ordering methods, which select only black as the reference color for sorting pixels, result in the problem in which the scope of the distance measurement is not optimal. The proposed ARCS scheme is used for determining the ideal reference color for MM and for color image segmentation application. In addition, we use both 1D histogram-based modeling scheme binning from 3D color spaces, such as red–green–blue and hue–saturation–intensity, and 2D color models, such as (H, S), (Cb, Cr), and (I, By). According to the results of the quartile analysis, the threshold determination reacts with less sensitivity to the context variations of the images tested. The experiments focused on color-based image segmentation using the proposed ARCS scheme for color MM processing through a bottom–up scenario. To evaluate the system, four quantitative indices were utilized for an ARCS comparison using advanced segmentation methods in the experiments. The cross validation with different system parameters and a comparison of the morphological gradient operation with different color models are also presented.**

***Index Terms*— Adaptive mathematical morphology, color image segmentation, kernel density estimation, reference color selection, region growing, region merging.**

I. Introduction

IN THE PAST decade, mathematical morphology (MM) [1]–[3] has been widely applied in image processing such as image retrieval [4], satellite imagery [5], template matching [6], [7] aerial surveillance [8], [9], and image segmentation [10]–[13]. Such high-dimensional image data have facilitated the extension of MM from binary and gray-scale to color images, and even higher dimensions of visual features [14], [15]. This is crucial for the continual development of image processing, which tends to consider only the illumination information of pixels. However, the task of MM typically neglects the details of the image content. Because acquisition techniques for color images continue to advance and mature, their compatibility with extant algorithms should be extended, and must be as concrete as possible.

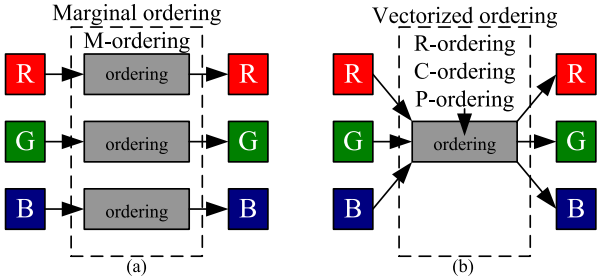

Fig. 1. Two approaches of the color morphological processing. (a) Marginal ordering, (b) vectorized ordering.

Managing a color image implies that the dimension increment of a feature vector and the computational complexity result in a longer execution time compared with manipulating a gray-scale image. In high-dimensional space, the interchannel correlation increases, reducing the computational cost and severing the correlation between channels challenging. MM has recently become widely used in image processing because of the advantage presented by set theory. Adaptive MM facilitates the application of high-dimensional image data, which can be extended from binary and gray-scale images to color images, and even to higher dimensions of visual features.

The MM process is an application based on lattice theory in spatial structures [16]. Understanding the relationship between pixels and sorting them according to their characteristics becomes crucial. However, ranking higher-dimensional vectors in a direct manner remains a challenge. Compared with a single-dimensional image (e.g., binary and grayscale), no standard ordering mechanism exists for color feature vectors. Color ordering for color morphological processing can typically be divided into two approaches: marginal- and vector-oriented methods (**Fig. 1**). The marginal-oriented approach involves operating each color component independently. In other words, the ordering method does not consider the marginal correlation between components, and treats each color component as a gray-scale image. By contrast, the vector-oriented approach performs color morphology as a vectorized ordering mechanism including reduced ordering,

Manuscript received May 7, 2015; revised August 20, 2015 and November 24, 2015; accepted December 22, 2015. Date of publication June 30, 2016; date of current version August 19, 2016. This work was partially supported by Ministry of Science and Technology of Taiwan (MOST), under grant MOST 103-2221-E-155-027-MY2. The associate editor coordinating the review of this manuscript and approving it for publication was Prof. Jing-Ming Guo. *(Corresponding author: Huang-Chia Shih.)*

The authors are with Human-Computer Interaction Multimedia Laboratory, Department of Electrical Engineering, Yuan Ze University, Taoyuan 320, Taiwan (e-mail: hcshih@saturn.yzu.edu.tw; royal.shih@gmail.com).

Color versions of one or more of the figures in this paper are available online at http://ieeexplore.ieee.org.

Digital Object Identifier 10.1109/TIP.2016.2586658

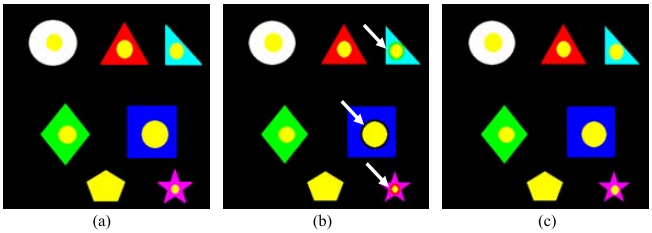

Fig. 2. M-ordering suffers from false color (e.g. pointing by white arrows). (a) Original image, (b) erosion results using M-ordering, (c) erosion results using R-ordering.

conditional ordering, and partial ordering. Numerous recent studies have proposed sequential ordering approaches of color morphology, which can be categorized into the following four fundamental modes.

A. Marginal Ordering (M-Ordering)

The M-ordering method, as shown in **Fig. 1(a)**, ranks each component of channels individually, and ignores any interrelationship between channels. In an example of the M-ordering morphological erosion process, a ring-like junction with false colors emerges between the inside circle and the geometric shape, as shown in **Fig. 2(b)**. This frequently results in the appearance of a false color, meaning that this new color is absent in the original image. This type of method is thus evidently inefficient and infeasible for use. Chunjiang [17] proposed a modified M-ordering method, which considered each feature of a channel for sorting their sequential order to avoid the generation of a false color.

B. Reduced Ordering (R-Ordering)

The R-ordering approach is the most general ranking method and is based on the dimension reduction algorithm for mapping high-dimensional data onto low-dimensional data. The rank comparison is subsequently used for measuring the ordering relationship. The most popular methods using the R-ordering approach are distance mapping and principle component analysis. The authors in [18] introduced a vector median filter and a basic vector directional filter based on two R-ordering methods, and applied them to a color image. These filters enabled the system to reduce noise and maintain valid color information. The authors in [19] proposed a hyperspectral image-processing application based on supervised R-ordering. The advantage of the R-ordering approach is the ability to perform a morphological operation in reduced dimensions, which lowers the computational complexity. Nevertheless, this dimension reduction leads to color information loss, and generates ambiguous conditions during the rank comparison process. For example, the two color pixels p and q are in a hue–saturation–intensity (HSI) color space. To compute the distances from the color pixels to the reference color, c_{ref} comprises $D_{\mathrm{HSI}}(p, c_{ref})$ and $D_{\mathrm{HSI}}(q, c_{ref})$ respectively; thus, we obtained $D_{\mathrm{HSI}}(p, c_{ref}) = D_{\mathrm{HSI}}(q, c_{ref})$. As shown in **Fig. 3**, we may encounter ambiguous conditions when the order judgment is applied for these two color pixels, consequently reducing the confidence of order ranking and increasing the probability of an improper color assignment.

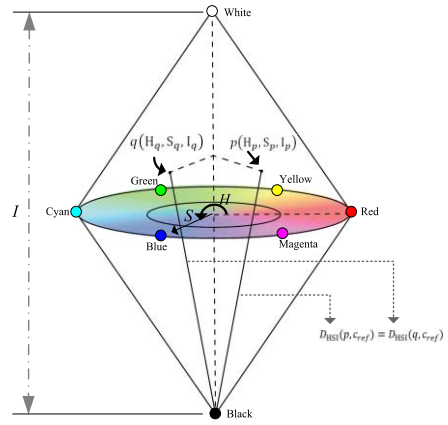

Fig. 3. Ambiguous condition for R-ordering while the black being used.

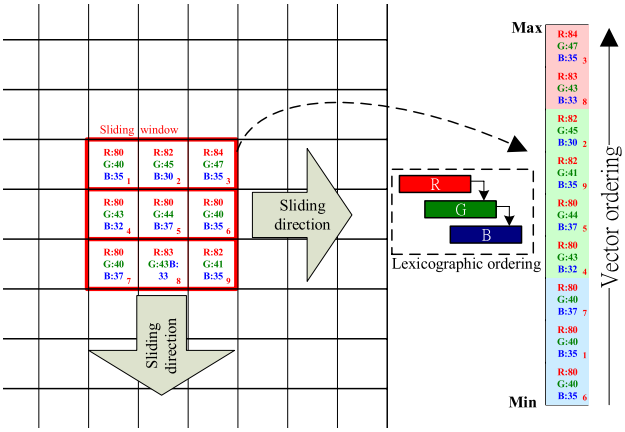

Fig. 4. An example of the lexicographic ordering.

C. Conditional Ordering (C-Ordering)

The C-ordering method, also known as lexicographic ordering, is based on a specific condition for comparing the component of a feature vector, which sets priorities between changes, and compares the order of each component in a stepwise manner. This approach enables the system to entirely avoid ambiguous conditions that are generated by the sequential comparison error. However, this ordering method requires the comparison of each channel, resulting in relatively high computational complexity. **Fig. 4** shows an example of lexicographic ordering, where each color vector of the structural elements is sorted according to the values. For the mechanism, the comparative order of the subjects is as follows: 1) Identify the values of the red component; 2) when the values of the red component are equal, compare the values of the green component; and 3) when the values of the green component are equal, compare the values of the blue component. Aptoula and Lefèvre [20] reported the merits and disadvantages of this type of method, and applied it in the morphological processing of color image noise reduction and color texture classification, and obtained satisfactory results.

D. Partial Ordering (P-Ordering)

The P-ordering approach [21] is a clustering-based scheme for which a vector partitioning approach is used. By using the information of the clusters, this approach allows the system

to conduct ordering according to the weight of the vector and its extremeness. Evans [22] proposed a novel ranking method based on the P-ordering scheme, which ranked each pair of vectors in groups of a higher or lower order. It is efficient for simply reducing vector-ranking complexity. This type of methodology basically compares the rank relationship of each pair of vectors, and is thus called "pairwise vector ordering."

In addition to these four ordering mechanisms, studies have presented algorithms designed from other viewpoints. For example, Lezoray et al. [23] presented a graph-based ordering method, in which they considered the structure element (SE) as a complete graph, with each vertex on it representing a pixel in an image. A weighted factor was assigned to each edge in the graph, after which the minimum spanning tree method was used for ranking the element of the vector. Several other studies [24]–[28] have proposed composite ranking methods including R+C ordering, P+M ordering, and bit-mixing ordering in MM processing for a color image.

The present study proposes an automatic reference color selection (ARCS) mechanism, which enables the management of diverse color models while increasing the ability to measure the distinction between color vectors. In adopting this mechanism, certain considerations are required. For example, the binning scheme may contain the sparse population problem because of the image size. The color histogram has numerous nonexisting colors beyond the gamut of photos, but only a few pixels are present per bin, with the position of the maximum most likely to be dominated by noise. To resolve this problem, we utilized the kernel density estimation (KDE) method [29], [30] to identify the definite dominant color. In addition, we propose an adaptive merging algorithm that does not require threshold determination. This improves the region-merging process in a simple and more convincing manner. We also propose a novel automatic threshold determination method for region-merging process by conducting quartile analysis.

The main contributions of this study include improvements in image segmentation through the use of the proposed ARCS scheme and the hybrid ordering method in addressing region merging [31], [32]. The efficiency of morphological ordering depends heavily on the distribution of image color. We adopted the complementary color of the dominant color of the test region as the reference color. The proposed algorithm is suitable for further semiautomatic image segmentation application [33], [34] as long as the merging criteria are defined. In addition, according to quartile analysis, the threshold determination reacts with less sensitivity to the context variations of the tested image. The burden of threshold determination is avoided substantially, enabling an authentic segmentation result to be achieved.

The remainder of this paper is organized as follows. Section II introduces the proposed ARCS and color-ordering scheme in the adaptive MM. Section III presents the details of the MM-based image segmentation algorithm. Section IV provides the experimental results. Finally, Section V offers a discussion of our findings and a conclusion.

II. Color-Based Adaptive MM Scheme

A. Color Representations and Color Distances

A typical color model used in image processing is the red–green–blue (RGB) representation. However, the RGB model has from an intrinsic disadvantage: a high correlation between color channels. In addition, it cannot be used to obtain the original intensity information of the image for reducing the computational burden during image acquisition. To overcome this limitation, we used color models that decouple the intensity component from the color-carrying information such as HSI and YCbCr. Furthermore, we adopted log-opponent chromaticity (i.e., I-By) representation [35] for our study. Regarding the log-opponent chromaticity space, Tan et al. [36] reported high accuracy in skin detection despite wide variations in ethnicity and illumination. The results showed that the spaces of (I, By) and (H, S) were comparable; however, (I, By) performance yielded a higher true-positive rate and a lower false-negative rate compared with (H, S). In addition, two major problems must be solved: 1) color distributions depend on the illumination color, and 2) when represented as histograms, the number of bins they are large, thus limiting the scale of bins that might reasonably be indexed. Because the correlations among components in these color spaces are essentially independent, we can manage each channel individually. This model provides a desirable property for vectoring the color image, and the chroma and brightness information can be considered mutually independent.

In color representation, we adopted a 1D histogram-based model from 3D color space such as RGB and HSI, and also used a 2D color model such as (H, S), (Cb, Cr), and (I, By). The statistical histogram $h(j)$ of image f is obtained by solving (1), as follows:

$$h(j) = \sum_i \delta\left[L_z(c_i) - j\right], \quad \text{for } 0 \le j \le n, \quad \forall c_i \in f \quad (1)$$

where $\delta(\cdot)$ denotes the Kronecker delta function (i.e., $\delta(\mathrm{x}) = 1$ for $\mathrm{x} = 0$; $\delta(\mathrm{x}) = 0$ otherwise), $L_z(c_i)$ denotes the binning function for pixel c_i in color model z, which enables the 3D HSI color model to transform as a ρ-bit value, totaling $n = 2^\rho$ bins, and j denotes the bin index of the color histogram. In this study, we used $\rho = 8$ bits, where 4 bits were from the H component, and 2 bits were each from the S and I components. Otherwise, when $z = \{(\mathrm{H}, \mathrm{S}), (\mathrm{Cb}, \mathrm{Cr}), (\mathrm{I}, \mathrm{By})\}$, we employed a 2D histogram with 256-by-256 bins.

Because the dimension of the color space is mostly larger than 1, it is critical to determine the actual relationship between the value of the color distance and the awareness of the human eye. The International Commission on Illumination (CIE) defines a distance metric Delta-E (*dE*), which is a single number that represents the distance between two colors. When a *dE* of 1.0 is the smallest color difference discerned by the human eye, a *dE* less than 1.0 is imperceptible. However, certain color differences greater than 1 are acceptable, despite perhaps being unnoticeable. The major problem of *dE* involves resolving the perceptual uniformity issue inadequately. A certain *dE* that may be meaningless between two colors because it cannot be perceived may be conspicuous in another part of

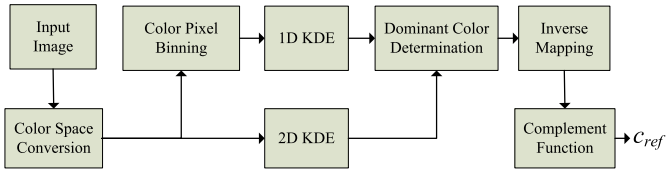

Fig. 5. Schematic diagram of the proposed ARCS scheme.

the spectrum. The CIE constantly corrects and modifies this benchmark to produce *dE*76, *dE*94, and *dE*2000. In addition, *dE*2000 is the first major revision of the *dE*94 equation. Unlike *dE*94, which assumes that L* (where the L*a*b* color space) correctly reflects the perceived differences in lightness, *dE*2000 varies the weighting of L* depending on where in the lightness range the color falls. The *dE*2000 equation is still under consideration and does not seem to be widely supported in graphical arts applications. The equation is also useful for *dE* measurements when an image includes many layered colors such as the fading effect. This is a rare condition for natural images. Consequently, the use of the *dE* color distance for image segmentation is negligible.

Numerous color distance measurements have recently been proposed. An improved survey of different distance measures for vector filters was reported by Celebi [37]. The results of image segmentation with different distance measures evidently differ, but the focus of our ARCS algorithm is on the color spaces and ordering algorithm. In the current study, in addition to the RGB and HSI color models, we used the norm-2 Euclidean distance measure to perform pixel and region similarity. Let D_z denote the color distance in color model z. In practice, the distance measures are used for measuring the distinction between the tested color and reference color.

B. Automatic Reference Color Selection Scheme

There is scant, if any, literature on selecting the reference color c_{ref}. A schematic diagram of the proposed ARCS scheme is shown in **Fig. 5**. The major criterion for color selection theoretically entails selecting the pixel that is most distant from the tested color pixel. It represents the distinguishing ability between two color pixels. Numerous researchers (e.g., [16], [23], [25]) have simply employed black as the reference color. However, this leads to the problem in which the scope of the distance measurement is not optimal; that is, the efficiency of ordering depends heavily on the distribution of the image color. To address this problem, we considered the color distribution of the image to determine the dominant color. The most appropriate reference color is selected using the complementary color of the dominant color. This method evidently yields the distance measure for achieving the highest discriminative ability.

Nevertheless, histograms are a common strategy for representing medium-size color distributions in 1D or 2D space. Because of the limited image size, it is possible to form sparse bins and few pixels per bin for the histogram. Consequently, the peak of the histogram is dominated by noise. To rectify this defect, kernel density estimation (KDE) is an alternative approach for determining the dominant color.

A KDE is a nonparametric graph that can reconstruct an unknown population from a random data sample. The KDE does not use regression for fitting a distribution to the data. The simple concept underlying kernel estimates is that each bin j_w, $w = 1, 2, \ldots, n$ is drawn from an unknown density histogram $h(j)$, which is replaced by a specified distribution (e.g., normal), centered on the point, and with a standard deviation designated by a smoothing parameter h_s (called the bandwidth, and $h_s > 0$). We were interested in estimating the shape of this function h. Its kernel density estimator can be expressed as

$$\hat{h}(j) = \frac{1}{nh_s} \sum_{w=1}^{n} \emptyset_{h_s}\left(\frac{j - j_w}{h_s}\right), \quad \text{for } 0 \le j \le n \tag{2}$$

where $\emptyset(\cdot)$ denotes the kernel (i.e., standard normal kernel in this paper), a non-negative function that is integrated to one and has mean zero; that is,

$$\emptyset_{h_s}(x) = \frac{1}{\sqrt{2\pi}h_s} \exp\left(-\frac{x^2}{2h_s^2}\right). \tag{3}$$

Finally, the bin with the maximal value computes the complementary color to serve as the reference color; that is,

$$j^* = \arg_j \max_{S_x} \{\hat{h}(j)\}, \quad \text{for } \forall j \tag{4}$$

and

$$c_{ref} = \mathrm{C}\left(L_z^{-1}(j^*)\right), \tag{5}$$

where j^* denotes the bin of the histogram with the maximal value; $L_z^{-1}(\cdot)$ denotes the reverse mapping function, which is used for obtaining the z color model from the input bin; and C denotes the complementary color regarding the color model. For example, when the color model includes illumination information, the complementary color is selected from the mirror at the origin. By contrast, the definition of the regular complementary color is adopted. When the dominant color is located exactly on the SI plane, we simply consider black as the reference color. However, the KDE method is performed for modeling the density of color distribution, and the densest color may be absent in the original color palette. Hence, a predefined circular boundary S_x ranging from the center of the peak density is used to determine the dominant color.

C. Hybrid Color-Ordering Algorithm

This paper proposes a hybrid color-ordering (HC ordering) method, which takes advantage of R- and C-ordering. This method sustains the advantages of R-ordering by reducing the dimension of the feature vector to lower the computational cost, but also avoids the ambiguous condition generated by C-ordering when measuring the importance of the color vector. In addition, the reference color c_{ref} can be determined using the proposed ARCS scheme. The HC-ordering approach is detailed in the following steps.

1) Global Ranking: R-ordering is a color-ranking operation based on the distance between the color of the pixel under resting and the reference color projected onto the color space:

$$c_p <_{c_{ref}} c_q \Longleftrightarrow \left\|c_p - c_{ref}\right\|_{D_z}^{z} > \left\|c_q - c_{ref}\right\|_{D_z}^{z} \tag{6}$$

where c_p and c_q denote two pixels with different color components, "$\Longleftrightarrow$" denotes an "if and only if" relationship, $<_{c_{ref}}$ denotes the pixel-based comparison operator with the selected reference color c_{ref}, $\|\cdot\|_{D_z}^{z}$ denotes the color distance measurement D_z, and the superscript z denotes the used color model, where $z \in \{(R, G, B), (H, S, I), (Cb, Cr), (H, S), (I, By)\}$.

2) Local Ranking: C-ordering is employed for avoiding ambiguous conditions. For example, if two color pixels have different color components in a color space, but the distance from the reference pixel is identical, then the result is that they are classified as the same color. To prevent this problem, the proposed HC-ordering algorithm considers the C-ordering method. This method has also been called lexicographical ordering, and is expressed as

$$c_p <_{HC} c_q \Longleftrightarrow \begin{cases} \left\|c_p - c_{ref}\right\|_{D_z}^{z} > \left\|c_q - c_{ref}\right\|_{D_z}^{z} \\ \quad \cup \left\|c_p - c_{ref}\right\|_{D_z}^{z} \leq \left\|c_q - c_{ref}\right\|_{D_z}^{z} \\ \cap \begin{cases} c_p^1 < c_q^1 \\ \cap c_p^1 = c_q^1 \cap c_p^2 < c_q^2 \\ \cap c_p^1 = c_q^1 \cap c_p^2 = c_q^2 \cap c_p^3 < c_q^3 \end{cases} \end{cases} \tag{7}$$

where $c_p = (c_p^1, c_p^2, c_p^3)$ and $c_q = (c_q^1, c_q^2, c_q^3)$ represent two pixels with 3D color information, $\cup$ denotes the logical OR operator, and $\cap$ represents the logical AND operator.

The main concept of the C-ordering method involves sorting each color component with a specific ordering priority. A good priority of ordering depends on the context of images. It enables the system to obtain different results from morphological processing by adjusting the order of comparisons among the components. For example, when the dilation operation is applied to the RGB color space with the priority R→G→B, the red tone of the test image is expanded considerably. Conversely, when the priority G→R→B is adopted, the green tone is enhanced. However, the RGB color space is highly sensitive to the human eye; processing color values in the conventional manner results in an unreal and false color appearance. The HSI model of color takes advantage of how the human eye perceives colors; therefore, it is the most frequently adopted model for image-processing applications. For edge detection application, the priority of I→S→H is more appropriate compared with H→S→I, because the boundary of the object reflects the sharp change in intensity. Likewise, the human eye is sensitive to minor changes in intensity, but not with color. However, under the condition in which the color component is more critical compared with intensity (e.g., skin color tone detection), and one intends to depress the distortions caused by the flicker of the light source, the morphological operator tends to adopt the priority of H→S→I. This mechanism circumvents an increase in brightness sensitivity for color-oriented image-processing applications. Similarly, for the other color models, we adopted By→I, Cr→Cb, and H→S.

Fig. 6. Dilation and erosion operations, (a) original image, (b) M-ordering erosion, (c) M-ordering dilation, (d) HC-ordering erosion (SE=3, without ARCS), (e) HC-ordering erosion (SE=3, with ARCS), (f) HC-ordering erosion (SE=10, with ARCS), (g) HC-ordering dilation (SE=3, without ARCS), (h) HC-ordering dilation (SE=3, with ARCS), and (i) HC-ordering dilation (SE=10, with ARCS).

D. Color-Based MM Operators

According to the color distance and ordering scheme measurements, we can apply the primary operators of the color MM, the basic operators of which are erosion and dilation operators.

Definition 1 (Erosion and Dilation): The erosion of image f with an s-size structural element B on pixel x is defined as

$$\varepsilon_{HC,sB}(f)(x) = \{f(y) : f(y) = \wedge_{HC}[f(b)], b \in s(B_x)\}. \tag{8}$$

Similarly, the dilation of image f with the n-sized structure element B on pixel x can expressed as:

$$\tau_{HC,sB}(f)(x) = \{f(y) : f(y) = \vee_{HC}[f(b)], b \in s(B_x)\}. \tag{9}$$

where $\wedge_{HC}$ and $\vee_{HC}$ denote the infimum and supremum, respectively, in accordance with the proposed HC-ordering scheme. Examples of erosion and dilation are shown in **Fig. 6**.

In addition, numerous color MM operations can be performed by varying the combination of the erosion and dilation operators. In this paper, we explain only a few operators such as opening, closing, gradient, smoothing, and contrast enhancement.

Definition 2 (Opening and Closing): The opening operator is operated using erosion, followed by the dilation of image f. The main purpose is to eliminate patches with color peaks smaller than the structural element such that those closer to the reference color can be obtained.

$$\gamma_{HC,sB}(f) = \tau_{HC,nB}\left(\varepsilon_{HC,sB}(f)\right). \tag{10}$$

Conversely, the closing operator is operated using dilation, followed by the erosion of image f. The main purpose is

Fig. 7. Opening and closing operations. (a)Original image, (b) M-ordering opening, (c) M-ordering closing, (d) HC-ordering opening (SE=3, without ARCS), (e) HC-ordering opening (SE=3, with ARCS), (f) HC-ordering opening (SE=10, with ARCS), (g) HC-ordering closing (SE=3, without ARCS), (h) HC-ordering closing (SE=3, with ARCS), and (i) HC-ordering closing (SE=10, with ARCS).

to bridge gaps smaller than the structural element and those that are as distant as possible from the peak of the reference color.

$$\varphi_{HC,sB}(f) = \varepsilon_{HC,sB}\left(\tau_{HC,sB}(f)\right). \tag{11}$$

An example of the opening and closing operations is shown in **Fig. 7**.

Definition 3 (Gradient): The gradient reflects the status of the decline in intensity. The gradient value of a real object boundary is typically larger than that of the internal region. The purpose of the gradient operator is to generate a symbolic energy distribution of the information on the image texture. After the dilation operation for image f, and after subtracting using the eroded image, the remaining value of the gradient is the norm value, which is expressed as

$$\nabla_{HC}(f) = \left\|\tau_{HC,sB}(f) - \varepsilon_{HC,sB}(f)\right\|. \tag{12}$$

Definition 4 (Smoothing): Noise corruption in the image is the product of the false color pixel in the MM process as well as a result of false segmentation. Therefore, before conducting image segmentation, it is necessary to apply image smoothing. The morphological smoothing operator typically aims to suppress noise in the image from the opening and closing operations. This step eliminates impulse noise with efficiency. However, the resultant image is subjected to partial distortion. To resolve this problem, we adopted an alternate sequential filter (ASF) for the image-smoothing operation. This filter enhances noise management performance more than typical opening/closing operations do. The main objective was to discard the patches of the peak and valley that are smaller than the structural element. This results in noise reduction, which can be expressed as

$$\begin{aligned}&\mathrm{ASF}(f)_{HC,sB}\\ &\quad = \varphi_{HC,sB}\gamma_{HC,sB}\cdots\varphi_{HC,2B}\gamma_{HC,2B}\varphi_{HC,1B}\gamma_{HC,1B}(f).\end{aligned} \tag{13}$$

Definition 5 (Contrast Enhancement): The purpose of contrast enhancement is to enlarge the dynamic range of density distribution, which can stretch visual distinctions. For this paper, we employed color contrast mapping [23], which establishes a mapping relationship by conducting a comparison between original and eroded images against original and dilated images, respectively. This method evidently enhanced the image contrast and simultaneously suppressed image distortion. This operation enabled the system to enhance the contrast of the image and reduce its distortion, and is defined as

$$\kappa^{\varepsilon\tau}_{HC,sB}(f)(x) = \begin{cases}\tau_{\mathrm{HC},sB}(f)(x) & \text{if } \|f(x)-\tau(f)(x)\| \\ & \quad \le \|f(x)-\varepsilon(f)(x)\| \\ \varepsilon_{\mathrm{HC},sB}(f)(x) & \text{if } \|f(x)-\tau(f)(x)\| \\ & \quad > \|f(x)-\varepsilon(f)(x)\|.\end{cases} \tag{14}$$

III. Image Segmentation Based on the HC-Ordering

The formal procedure of bottom-up image segmentation includes two phases: 1) presegmentation using the color gradient image, which can first be obtained using the HC-ordering-based MM, and then watershed image segmentation for roughly segmenting the original image; and 2) regarding the region distance, the sequential regions are subjected to the merging scheme for segmentation.

A. Image Presegmentation

The purpose of this phase is to extract the initial partitions of the image by adopting the color gradient and watershed-based segmentation. The watershed-based algorithm is the one of the most efficient image segmentation methods, and was proposed by Vincent and Soille [38]. The main concept of the watershed algorithm involves adopting the original image as a stereo mountain diagram. The gradient energy is treated as the rise and decline of the mountain. Solving the region-merging algorithm yields the initial segmentation. According to our observations, performing split and merge to segment the image initially yields a performance that is identical to that of watershed segmentation. Therefore, we simply employed watershed segmentation as the presegmentation process.

B. Region Merging Using HC-Ordering

The conventional watershed method is subject to oversegmentation in a small region because of noise and complex image patterns. It reduces the performance of image segmentation substantially, and thus we propose a more robust region-merging algorithm. According to the concept of distance, the region-based MM was employed for determining the likelihood of merging between two adjacent regions.

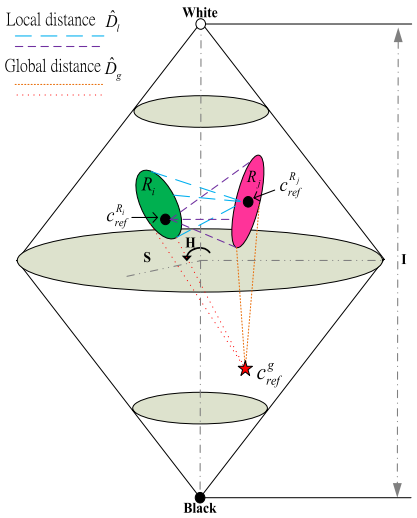

Fig. 8. Distance measure with global and local ranking.

Suppose that the initial partition of the region is performed through watershed segmentation, and is denoted as $S = (R_1, \ldots, R_n)$. The objective of image merging is to achieve a merger discrimination matrix P, which represents the result of the final segmentation. Afterward, the watershed image is tagged as the initial image, and the merging step is executed using the bottom-up scenario to operate a global search for the two tags (i.e., regions) with the minimum difference. This difference value represents the mean of the color distance D_g derived from the reference color, which uses the dominant color of the entire image (i.e., global rank), which are depicted by the red and blue dashed lines shown in **Fig. 8** (e.g., HSI color model). If we assume that $R_i = (p_1, \ldots, p_n)$ and $R_j = (q_1, \ldots, q_m)$ represent two groups of pixels in adjacent regions, the global distance of R_i can be computed with

$$\hat{D}_g\left(R_i, c_{ref}^g\right) = \frac{1}{n}\sum_{k=1}^{n} D_z\left(p_k, c_{ref}^g\right), \tag{15}$$

where D_z is the HSI distance, and c_{ref}^g can be obtained by solving (5), which indicates the global reference color. According to (6), the ranking relationship between the two regions of these average color distances can be measured through R-ordering as follows:

$$R_i <_{c_{ref}^g} R_j \Longleftrightarrow \hat{D}_g\left(R_i, c_{ref}^g\right) > \hat{D}_g\left(R_j, c_{ref}^g\right). \tag{16}$$

To avoid the ambiguous condition generated from R-ordering, the C-ordering scheme is applied in this system. From a local viewpoint, the difference value D_l is computed between these two adjacent regions. Specifically, we calculated the average color distance by using the dominant color as the reference color in the HSI color space, indicated by the dotted brown and green dashed lines shown in **Fig. 8**. The average color distance is defined as

$$\hat{D}_l\left(R_i, c_{ref}^{R_j}\right) = \frac{1}{n}\sum_{k=1}^{n} D_z\left(p_k, c_{ref}^{R_j}\right), \tag{17}$$

where $c_{ref}^{R_j}$ denotes the reference color regarding region R_j, which can be obtained by solving (5).

According to (16) and (17), the HC-ordering operation $<_{HC}^{R}$ can be derived from

$$R_i <_{HC}^{R} R_j \Longleftrightarrow \begin{cases} \hat{D}_g\left(R_i, c_{ref}^g\right) > \hat{D}_g\left(R_j, c_{ref}^g\right) \\ \cup\, \hat{D}_g\left(R_i, c_{ref}^g\right) \le \hat{D}_g\left(R_j, c_{ref}^g\right) \\ \cap \left\{\hat{D}_l\left(R_i, c_{ref}^{R_j}\right) < \hat{D}_l\left(R_j, c_{ref}^{R_i}\right)\right. \end{cases}. \tag{18}$$

Consequently, the merger discrimination matrix P can be constructed using the global threshold TH_g and local threshold TH_l.

$$\mathrm{P}(R_i, R_j) = \begin{cases} true & if\ \hat{D}_g(R_i, R_j) < TH_g \cap \hat{D}_l(R_i, R_j) < TH_l \\ flase & otherwise. \end{cases} \tag{19}$$

Empirically, TH_g can be adjusted using the entropy of the color distribution, and TH_l depends on the local probability density over the entire image. Finally, HC-ordering can be completed by determining the minimum difference value. When $\hat{D}_g\left(R_i, R_j\right)$ is less than the global threshold TH_g and $\hat{D}_l\left(R_i, R_j\right)$ is less than the local threshold TH_l, these two regions can be merged. The algorithm terminates when this difference value is larger than the predefined threshold.

C. Adaptive Threshold Determination

As mentioned, the HC-ordering method is required to determine a threshold value for managing region merging. For different images, a specific threshold is required. To resolve this issue, we performed quartile analysis for the adjacent regions, and determined an ideal threshold for merging.

1) Quartile Analysis: Quartile analysis is a statistical method [48], [49]. The quartiles of a ranked set of data values are three points that divide the data set into four equal groups. Consequently, each group comprises a quarter of the data and are distinguished by the points on 25%, 50%, and 75% of the highest value of the data set, represented as Q_1, Q_2, and Q_3, respectively. Furthermore, the value of $Q_1 - Q_3$ is called an interquartile range (IQR), which is typically applied for characterizing the data in the presence of extremities that may skew the data. The IQR is a relatively robust statistic compared with the range and standard deviation, and represents the distribution among 50% of the data set approaching the median value. To verify the existence of outliers and determine the "fences," quartiles can be used through the upper and lower limits of the data; that is, any observation is an outlier when it is outside the range of $[Q_1 - k(Q_3 - Q_1),\ Q_3 + k(Q_3 - Q_1)]$, where k denotes a nonnegative constant.

2) Region-Merging Algorithm Using Quartile Analysis: According to the quartiles of Q_1 and Q_3, we analyzed the distributions of two neighboring regions R_i and R_j. First, the values of the HSI color distance regarding the reference color c_{ref}^g were viewed as the data set for quartile analysis. Second, we obtained the values of Q_1, Q_2, and Q_3. Finally, we considered whether to merge the two regions R_i and R_j after observing the value of the IQR.

Here, we suppose that the number of pixels in R_i is greater than that in R_j. Four cases are met in quartile analysis as follows:

1) The HSI distance distribution of R_j is included completely in R_i; that is, $Q_1^g\left(R_j, c_{ref}^g\right) > Q_1^g\left(R_i, c_{ref}^g\right)$ and $Q_3^g\left(R_j, c_{ref}^g\right) < Q_3^g\left(R_i, c_{ref}^g\right)$. This indicates that the color distribution of R_j belongs to R_i. In this case, R_j and R_i can merge, and are assigned the highest priority for region merging.
2) The HSI distance distribution of R_j is partially included in R_i; therefore,
   a) $Q_1^g\left(R_j, c_{ref}^g\right) > Q_1^g\left(R_i, c_{ref}^g\right)$ and $Q_1^g\left(R_j, c_{ref}^g\right) < Q_3^g\left(R_i, c_{ref}^g\right)$, or
   b) $Q_3^g\left(R_j, c_{ref}^g\right) > Q_1^g\left(R_i, c_{ref}^g\right)$ and $Q_3^g\left(R_j, c_{ref}^g\right) < Q_3^g\left(R_i, c_{ref}^g\right)$.

   This shows that a part of the color distribution of R_j is included in R_i. In this case, R_j and R_i are enabled to merge, but with a second priority.
3) The HSI distance distribution of R_j is excluded from R_i. However, the distribution range of R_j is still located in the maximum and minimum observation values of R_i (i.e., 1.5 times the IQR). Therefore, it satisfies the following conditions:
   a) $Q_1^g\left(R_j, c_{ref}^g\right) > Q_{1-1.5\mathrm{IQR}}^g\left(R_i, c_{ref}^g\right)$
   b) $Q_1^g\left(R_j, c_{ref}^g\right) < Q_{3+1.5\mathrm{IQR}}^g\left(R_i, c_{ref}^g\right)$
   c) $Q_3^g\left(R_j, c_{ref}^g\right) > Q_{1-1.5\mathrm{IQR}}^g\left(R_i, c_{ref}^g\right)$
   d) $Q_3^g\left(R_j, c_{ref}^g\right) < Q_{3+1.5\mathrm{IQR}}^g\left(R_i, c_{ref}^g\right)$

   This indicates that the color distribution of R_j does not belong to R_i; however, it remains within the tolerant range for R_1. In this case, R_j and R_i are permitted to merge, but with a third priority.
4) The HSI distance distribution range of R_j is excluded completely in R_i, but is also outside of the maximum and minimum observation values of R_i (i.e., 1.5 times the IQR). This shows that the pixels in R_j and R_i are completely different. Basically, these two regions cannot be merged in this case.

According to these four cases and priorities, we used a bottom-up scenario to merge a region with fewer pixels with another region with more pixels until convergence was reached. Here, we computed the color distance between each segmented region and the global reference color c_{ref}^g to determine the merging priorities. To ensure accuracy in the merging process, we considered the local property of the image. By verifying whether the local color distance between adjacent regions exceeded the IRQ of the observation range by 1.5 times, ambiguity problems can be avoided only if the global distance measure is used. In summary, we employed quartile analysis to determine the data distributions.

IV. Experimental Results

To evaluate the performance of the proposed method, the images under testing were adopted from the Berkeley Segmentation Dataset [39]. We used four standard indices to quantitatively evaluate the performance of the proposed method. The experiments were performed to 1) determine the effectiveness of the different system parameters; 2) compare the morphological gradient operation with different color models; and 3) compare the results of the HC-ordering scheme with advanced methods in image segmentation application, including SAS [40] and SLIC superpixels [41]. In addition, typical methods such as the marker-controlled watershed method [42] and the mean-shift clustering method [43] were also used for our comparison.

A. Measures of Objective Evaluation

For this study, we used four indices to evaluate the quantitative comparison of typically used methods, including the Normalized Probabilistic Rand index (NPRI) [44], variation of information (VoI) [45], global consistency error (GCE) [46], and boundary displacement error (BDE) [47]; the property of the NPRI differs from those of the other three indices. A higher value of the NPRI signifies improved performance.

1) NPRI: The Probabilistic Rand index (PRI) evaluates the performance of the segmentation result with respect to the ground-truth image. The NPRI is an extension of the PRI, which yields a meaningful comparison of scores between segmented and ground-truth images.

2) VoI: The VoI is based on the relationship between the pixel and its cluster, and is used for determining the distance between a certain segment and another segment by employing a common information metric and conditional entropy. The VoI has been used for measuring changes in information between segmented and ground-truth images. A smaller value of VoI represents a lesser degree in the amount of information that can be changed. In other words, it represents the actual segmented result being closer to the referenced ground-truth image.

3) GCE: The GCE is an error measure that is used for quantifying the consistency between image segmentations. This index computes the probability of any two partitions that can be classified as the same subimage at different scales. Specifically, this index computes the probability of any two segments that can be classified as the same subimage at different scales. If the GCE value is small, this indicates fewer image segmentation errors.

4) BDE: This index computes the average offset error of a boundary pixel between two segmented regions. It defines the error in the distance between a certain pixel on the boundary and the closest boundary pixels in another segment.

B. Cross-Validation of System Sensitivity

To analyze the robustness of the system, we verified the reliability of the proposed system by using diverse system parameters. **Table 1** lists the parameters used in this experiment. **Table 2** lists the experimental results of the different parameters used for testing the segmentation accuracy.

TABLE I

DIFFERENT PARAMETERS APPLIED TO THE HC-ORDERING SEGMENTATION ALGORITHMS

Approaches	ARCS	Distance measure D_z	Color model z
The proposed	YES (c^g_{ref}= complement of dominant color)	HSI distance	HSI
Without ARCS	NO (c^g_{ref} = black)	HSI distance	HSI
Using Euclidean distance	NO (c^g_{ref} = black)	Euclidean distance	HSI
Using RGB color space	NO (c^g_{ref} = black)	Euclidean distance	RGB

TABLE II

COMPARISON OF DIFFERENT PARAMETERS FOR THE HC-ORDERING SEGMENTATION ALGORITHMS

Approaches	Performance Evaluation							
	NPRI [44]		VoI [45]		GCE [46]		BDE [47]	
	Rank1	*Rank2*	*Rank1*	*Rank2*	*Rank1*	*Rank2*	*Rank1*	*Rank2*
The proposed	**120(40.0%)**	**279(93.0%)**	**96(32.0%)**	**285(95.0%)**	**12(4.0%)**	**91(30.3%)**	**119(39.7%)**	**293(97.7%)**
Without ARCS	97(32.3%)	222(74.0%)	78(26.0%)	227(75.7%)	11(3.7%)	74(24.7%)	95(31.7%)	233(77.7%)
Using Euclidean distance	81(27.0%)	193(64.3%)	66(22.0%)	192(64.0%)	9(3.0%)	60(20.0%)	82(27.3%)	198(66.0%)
Using RGB color space	59(19.7%)	136(45.3%)	47(15.7%)	135(45.0%)	7(2.3%)	42(14.0%)	58(19.3%)	143(47.7%)

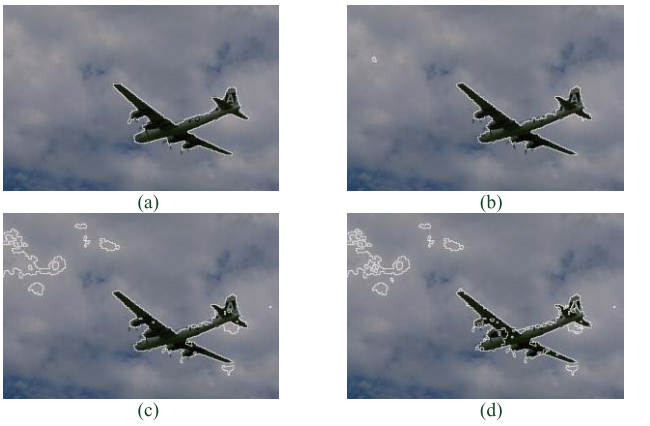

Fig. 9. Image segmentation results with the best thresholds: *airplane*, (a) the proposed HC-ordering (**TH_I=0.65**), (b) HC-ordering without ARCS (**TH_I=0.50**), (c) using Euclidean distance (**TH_I=0.55**), (d) using RGB color space (**TH_I=0.55**).

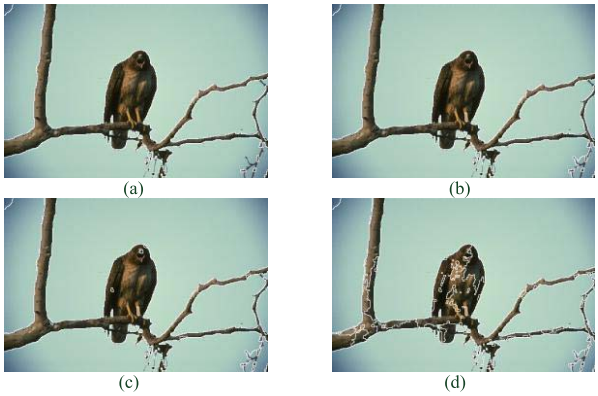

Fig. 10. Image segmentation results with the best thresholds: *hawk*, (a) the proposed HC-ordering (**TH_I=0.75**), (b) HC-ordering without ARCS (**TH_I=0.60**), (c) using Euclidean distance (**TH_I=0.55**), (d) using RGB color space (**TH_I=0.60**).

The most desirable performance is attained when the ARCS is applied in the HC-ordering scheme, whereas the least desirable performance occurs because of high interchannel correlation in the RGB color space, which causes ranking errors among the vectors. When the HSI color model is used, a consistent result considering human perception can be obtained. A stronger performance is obtained with the HSI distance measurement compared with the Euclidean distance measurement. Evidence of a robust performance of the proposed method is presented in **Figs. 9** and **10**.

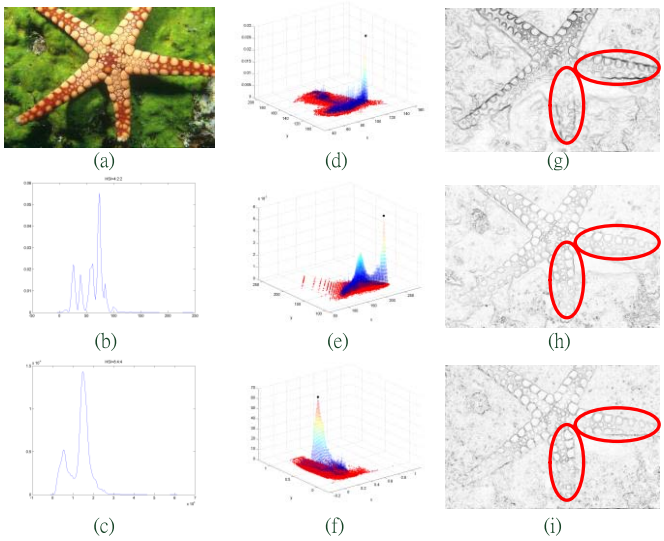

Fig. 11. Morphological gradient image: *starfish*, (a) original image (b)-(c) the histogram using 1D KDE with HSI 4-2-2 and 8-4-4 binning approaches, (d)-(f) the distribution map using 2D KDE in the (Cb, Cr), (I, By), and (H, S) color models, respectively, (g)-(i) the gradient images in the (Cb, Cr), (I, By), and (H, S) color models, respectively.

C. Comparison of Morphological Gradient Operation

For this experiment, we performed the morphological gradient by using the proposed ARCS and gradient operator, as shown in (12). The gradient of the image can be modeled using the derivative between neighbor pixels. For the gradient image, the region-merging algorithm can be used. **Figs. 11** and **12** display the obtained morphological gradients in different color models for the natural images. As shown in

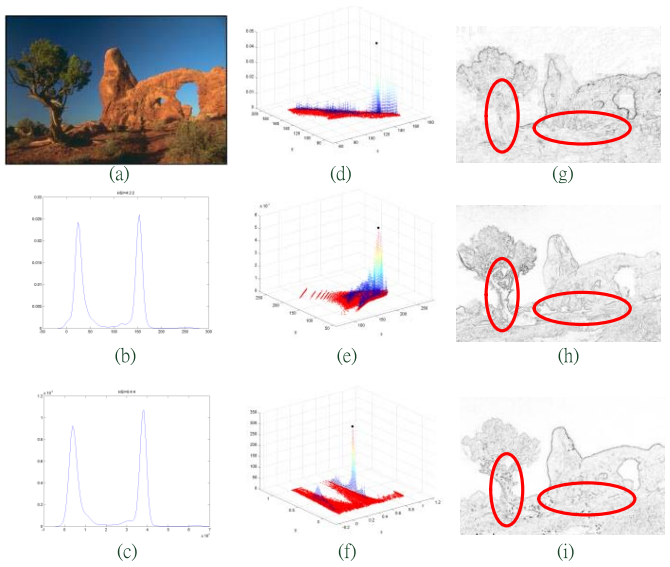

Fig. 12. Morphological gradient image: *Rock*, (a) original image (b)-(c) the histogram using 1D KDE with HSI 4-2-2 and 8-4-4 binning approaches, (d)-f) the distribution map using 2D KDE in (Cb, Cr), (I, By), and (H, S) color models, respectively, (g)-(i) the gradient images using (Cb, Cr), (I, By), and (H, S) color models, respectively.

Figs. 11(b) and **11(c)** as well as **12(b)** and **12(c)**, the binning approaches with 8 bits and 16 bits yielded similar distributions in 1D KDE. To avoid the sparse population condition and enhance modeling efficiency, we employed 2D modeling in this study. **Fig. 11(d)–11(f)** and **Fig. 12(d)–(f)** present the results of 2D KDE. The (I, By) color model yielded the most compact and highest dynamic distributions. As shown in **Figs. 11(g)–(i)** and **12(g)–(i)**, the gradient of the (Cb, Cr) color model contained the oversaturation problem in the boundary, and certain details were missing. Moreover, the gradient of the (H, S) color model was similar to that of the (I, By) color model; however, certain details are obscured in the starfish example shown in **Fig. 11**, and bimodel distribution is evident in the (I, By) color space. The original image in **Fig. 11(a)** shows that the color is strongly distinctive between the starfish and background seaweed. Similarly, the red circles in **Figs. 11** and **12**, representing the results of (I, By), show that it outperformed the color models (H, S) and (Cb, Cr).

D. Comparisons With Typically Used and Advanced Methods

Section III.C presents the region-merging algorithm based on quartile analysis. This method circumvents the threshold determination problem of the HC-ordering method, which is replaced by the characteristics of the data cluster to select a suitable threshold. Here, two typical segmentation methods were replicated and used for system evaluation. **Fig. 13** shows our quantitative comparison through a radar chart, revealing that the overall performance of HC-ordering (with hard threshold TH_l= 0.65) and the quartile-based method was more homogeneous compared with the other two methods. According to the results of our quantitative evaluation (**Fig. 13**), the proposed HC-ordering scheme outperformed the NPRI, VoI, and BDE approaches. However, the evaluation with

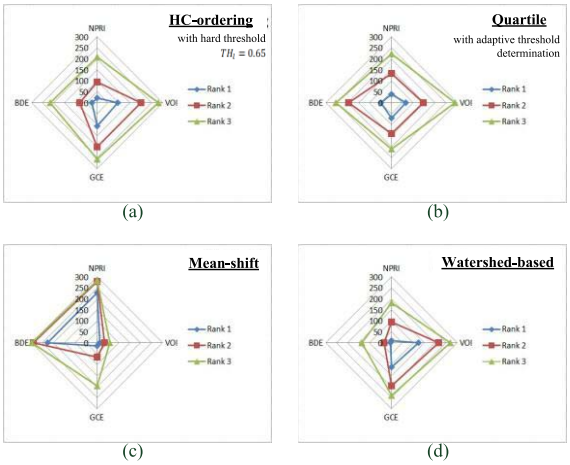

Fig. 13. Comparison of image segmentation through a radar chart. (a) HC-ordering method, (b) quartile method (c) mean-shift clustering method (d) Watershed method.

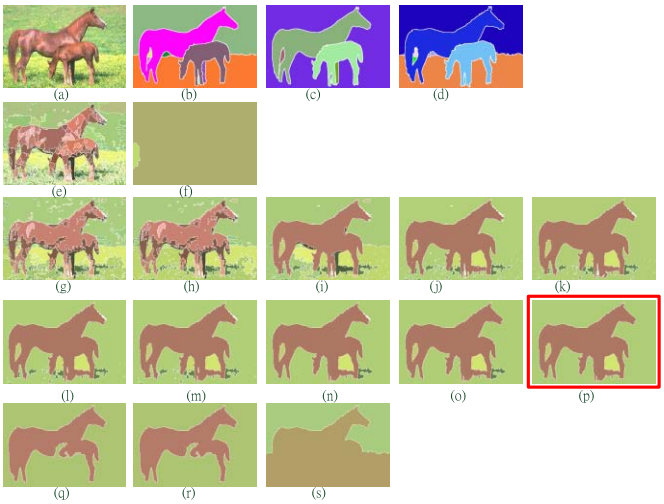

Fig. 14. Image segmentation results: *horse*. (a) Original image, (b)-(d) ground truth boundary, (e) mean-shift clustering method, (f) Marker Watershed method, (g)-(s) HC-ordering result for different thresholds (i.e., TH_l = 0.2, 0.25, 0.3, 0.35, 0.4, 0.45, 0.5, 0.55, 0.6, 0.65, 0.7, 0.75, 0.8), where the best result is $TH_l = 0.65$ with red-boxed.

GCE lacked effectiveness because the complex details affected the performance of the color-based ordering algorithm in color distinction. The mean-shift clustering method yielded outstanding results in the NPRI and VoI evaluations, but was limited in terms of the segmented images in the subjective evaluation. Overall, the performance of the proposed HC-ordering scheme was moderate, but it was more consistent with subjective human perceptions compared with the mean-shift clustering method. It was more salient in regions with small patches, and oversegmentation rarely occurred. **Figs. 14** and **15** show two images that were tested for our method comparison against two typically used segmentation methods. The proposed HC-ordering scheme obtained the most convincing segmentation results, and the segmentation boundaries were visually closer to the ground truth. The local threshold TH_l for the region-merging algorithm was sensitive to the context of the tested image, and different images require a specific threshold such as 0.65 for an image of a horse (**Fig. 14**) and 0.75 for an image of a rock (**Fig. 15**).

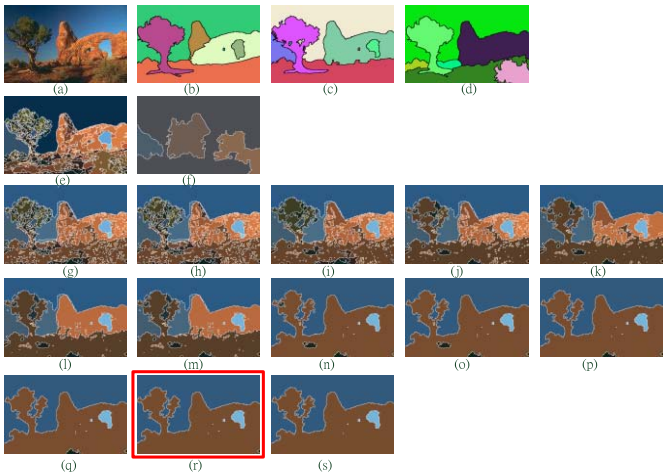

Fig. 15. Image segmentation results: *rock*. (a) Original image, (b)-(d) ground truth boundary, (e) mean-shift clustering method, (f) Marker Watershed method, (g)-(s) HC-ordering result for different thresholds (i.e., $TH_l = 0.2, 0.25, 0.3, 0.35, 0.4, 0.45, 0.5, 0.55, 0.6, 0.65, 0.7, 0.75, 0.8$), where the best result is $TH_l = 0.75$ with red-boxed.

TABLE III
COMPARISON OF COLOR IMAGE SEGMENTATION ALGORITHMS

Algorithms		Performance Evaluations over the Berkeley Segmentation Database			
		NPRI [44]	VoI [45]	GCE [46]	BDE [47]
SAS [40]		0.8319	1.6849	**0.1779**	11.29
SLIC superpixels [41]		0.8474	**1.5542**	N/A	11.15
Ours	z = (R, G, B)	0.8403	1.6134	0.2108	11.24
	z = (H, S, I)	0.8587	1.5947	0.1968	11.19
	z = (Cb, Cr)	0.8502	1.5991	0.2084	11.25
	z = (I, By)	**0.8639**	1.5624	0.1826	**11.13**
	z = (H, S)	0.8445	1.5885	0.1846	**11.14**

Two advanced segmentation methods were used for a comparison against the proposed method including SAS [40] and SLIC superpixels [41]. **Table 3** lists the quantitative results. By using different color models and distance measures, we found that the most desirable performance emerged when the log-opponent chromaticity (i.e., I-By) representation and norm-2 distance were used.

V. CONCLUSION

This article proposed an HC-ordering scheme combined with ARCS for determining the rank of color vectors and for discriminating the merger likelihood between two adjacent regions. The proposed ARCS scheme was used to determine the optimal reference color for MM and color image segmentation application. We also used 1D histogram-based modeling scheme binning from 3D color spaces such as RGB and HSI, and adopted 2D color models such as (H, S), (Cb, Cr), and (I, By). The experiments revealed that the segmentation result obtained using the (I, By) color model more accurately reflected subjective human perception. The presented adaptive merging algorithm with the ARCS scheme and HC-ordering algorithm used for MM-based image segmentation outperformed typical segmentation methods. We proposed an alternative method based on quartile analysis, and successfully avoided the HC-ordering method for an additional threshold determination step. This approach rendered region merging simpler and more practical.

REFERENCES

[1] E. Aptoula and S. Lefèvre, "On the morphological processing of hue," *Image Vis. Comput.*, vol. 27, no. 9, pp. 1394–1401, Aug. 2009.

[2] E. Aptoula and S. Lefèvre, "A comparative study on multivariate mathematical morphology," *Pattern Recognit.*, vol. 40, no. 11, pp. 2914–2929, Nov. 2007.

[3] J. Angulo, "Unified morphological color processing framework in a lum/sat/hue representation," in *Proc. Int. Symp. Math. Morphol. (ISMM)*, 2005, pp. 387–396.

[4] E. Aptoula and S. Lefèvre, "Morphological description of color images for content-based image retrieval," *IEEE Trans. Image Process.*, vol. 18, no. 11, pp. 2505–2517, Nov. 2009.

[5] M. Pesaresi and J. A. Benediktsson, "A new approach for the morphological segmentation of high-resolution satellite imagery," *IEEE Trans. Geosci. Remote Sens.*, vol. 39, no. 2, pp. 309–320, Feb. 2001.

[6] J. Weber and S. Lefèvre, "Spatial and spectral morphological template matching," *Image Vis. Comput.*, vol. 30, no. 12, pp. 934–945, Dec. 2012.

[7] H.-C. Shih and K.-C. Yu, "SPiraL Aggregation Map (SPLAM): A new descriptor for robust template matching with fast algorithm," *Pattern Recognit.*, vol. 48, no. 5, pp. 1707–1723, May 2015.

[8] H.-Y. Cheng, C.-C. Weng, and Y.-Y. Chen, "Vehicle detection in aerial surveillance using dynamic Bayesian networks," *IEEE Trans. Image Process.*, vol. 21, no. 4, pp. 2152–2159, Apr. 2012.

[9] H.-Y. Cheng and S.-H. Hsu, "Intelligent highway traffic surveillance with self-diagnosis abilities," *IEEE Trans. Intell. Transp. Syst.*, vol. 12, no. 4, pp. 1462–1472, Dec. 2011.

[10] I. Santillan, I. R. Terol-Villalobos, and G. Herrera-Ruiz, "Color morphological image segmentation on a new opponent color space based on the notion of critical functions," in *Proc. 7th Mexican Int. Conf. Artif. Intell. (MICAI)*, Oct. 2008, pp. 213–219.

[11] C. Meurie, O. Lezoray, L. Khoudour, and A. Elmoataz, "Morphological hierarchical segmentation and color spaces," *Int. J. Imag. Syst. Technol.*, vol. 20, no. 2, pp. 167–178, Jun. 2010.

[12] J. Yang, J. Liu, and J. Zhong, "Anisotropic diffusion with morphological reconstruction and automatic seeded region growing for color image segmentation," in *Proc. Int. Symp. Inf. Sci. Eng. (ISISE)*, vol. 2. Dec. 2008, pp. 591–595.

[13] M. A. Luengo-Oroz, E. Faure, and J. Angulo, "Robust iris segmentation on uncalibrated noisy images using mathematical morphology," *Image Vis. Comput.*, vol. 28, no. 2, pp. 278–284, Feb. 2009.

[14] A. G. Hanbury and J. Serra, "Morphological operators on the unit circle," *IEEE Trans. Image Process.*, vol. 10, no. 12, pp. 1842–1850, Dec. 2001.

[15] M. L. Comer and E. J. Delp, "Morphological operations for color image processing," *J. Electron. Imag.*, vol. 8, no. 3, pp. 279–289, Jul. 1999.

[16] J. Angulo, "Morphological colour operators in totally ordered lattices based on distances: Application to image filtering, enhancement and analysis," *Comput. Vis. Image Understand.*, vol. 107, nos. 1–2, pp. 56–73, Jul. 2007.

[17] Z. Chunjiang, "A new vectorial ordering for color morphology based on marginal ordering," in *Proc. 5th Int. Conf. Comput. Sci. Edu. (ICCSE)*, Hefei, China, Aug. 2010, pp. 1769–1772.

[18] R. Lukac, B. Smolka, K. Martin, K. N. Plataniotis, and A. N. Venetsanopoulos, "Vector filtering for color imaging," *IEEE Signal Process. Mag.*, vol. 22, no. 1, pp. 74–86, Jan. 2005.

[19] S. Velasco-Forero and J. Angulo, "Supervised ordering in IR^p: Application to morphological processing of hyperspectral images," *IEEE Trans. Image Process.*, vol. 20, no. 11, pp. 3301–3308, Nov. 2011.

[20] E. Aptoula and S. Lefèvre, "On lexicographical ordering in multivariate mathematical morphology," *Pattern Recognit. Lett.*, vol. 29, no. 2, pp. 109–118, Jan. 2008.

[21] M. C. d'Ornellas and J. A. T. B. da Costa, "Color mathematical morphology based on partial ordering of spectra," in *Proc. 20th Brazilian Symp. Comput. Graph. Image Process. (SIBGRAPI)*, Oct. 2007, pp. 37–44.

[22] A. N. Evans, "Nonlinear operations for colour images based on pairwise vector ordering," in *Proc. Digit. Imag. Comput., Techn. Appl. (DICTA)*, Dec. 2005, p. 61.

[23] O. Lezoray, A. Elmoataz, and C. Meurie, "Mathematical morphology in any color space," in *Proc. IEEE 14th Int. Conf. Image Anal. Process. Workshops (ICIAPW)*, Sep. 2007, pp. 183–187.

[24] P. Gonzalez, V. Cabezas, M. Mora, F. Cordova, and J. Vidal, "Morphological color images processing using distance-based and lexicographic order operators," in *Proc. 29th Int. Conf. Chilean Comput. Sci. Soc. (SCCC)*, Nov. 2010, pp. 258–264.
[25] J. Angulo, "Morphological color processing based on distances. Application to color denoising and enhancement by centre and contrast operators," in *Proc. IASTED Int. Conf. Vis., Imag., Image Process. (VIIP)*, Sep. 2005, pp. 314–319.
[26] A. R. Weeks and L. J. Sartor, "Color morphological operators using conditional and reduced ordering," in *Proc. SPIE Appl. Digit. Image Process. XXII*, vol. SPIE 3808. Oct. 1999, pp. 358–366.
[27] G. Louverdis, M. I. Vardavoulia, I. Andreadis, and P. Tsalides, "A new approach to morphological color image processing," *Pattern Recognit.*, vol. 35, no. 8, pp. 1733–1741, Aug. 2002.
[28] H.-C. Shih and E.-R. Liu, "Adaptive region merging approach for morphological color image segmentation," in *Proc. ACCV Workshop Feature Similarity Learn. Comput. Vis.*, Singapore, Nov. 2014, pp. 1–14.
[29] M. Rosenblatt, "Remarks on some nonparametric estimates of a density function," *Ann. Math. Statist.*, vol. 27, no. 3, pp. 832–837, 1956.
[30] E. Parzen, "On estimation of a probability density function and mode," *Ann. Math. Statist.*, vol. 33, no. 3, pp. 1065–1076, Sep. 1962.
[31] B. Peng, L. Zhang, and D. Zhang, "Automatic image segmentation by dynamic region merging," *IEEE Trans. Image Process.*, vol. 20, no. 12, pp. 3592–3605, Dec. 2011.
[32] F. Calderero and F. Marques, "Region merging techniques using information theory statistical measures," *IEEE Trans. Image Process.*, vol. 19, no. 6, pp. 1567–1586, Jun. 2010.
[33] C. Panagiotakis, I. Grinias, and G. Tziritas, "Natural image segmentation based on tree equipartition, Bayesian flooding and region merging," *IEEE Trans. Image Process.*, vol. 20, no. 8, pp. 2276–2287, Aug. 2011.
[34] C. Panagiotakis, H. Papadakis, E. Grinias, N. Komodakis, P. Fragopoulou, and G. Tziritas, "Interactive image segmentation based on synthetic graph coordinates," *Pattern Recognit.*, vol. 46, no. 11, pp. 2940–2952, Nov. 2013.
[35] J. Berens and G. D. Finlayson, "Log-opponent chromaticity coding of colour space," in *Proc. Int. Conf. Pattern Recognit.*, vol. 1. Sep. 2000, pp. 206–211.
[36] W. R. Tan, C. S. Chan, P. Yogarajah, and J. Condell, "A fusion approach for efficient human skin detection," *IEEE Trans. Ind. Informat.*, vol. 8, no. 1, pp. 138–147, Feb. 2012.
[37] M. E. Celebi, "Distance measures for reduced ordering-based vector filters," *IET Image Process.*, vol. 3, no. 5, pp. 249–260, Oct. 2009.
[38] L. Vincent and P. Soille, "Watersheds in digital spaces: An efficient algorithm based on immersion simulations," *IEEE Trans. Pattern Anal. Mach. Intell.*, vol. 13, no. 6, pp. 583–598, Jun. 1991.
[39] *Berkeley Segmentation Dataset*, accessed on Mar. 11, 2015. [Online]. Available: http://www.eecs.berkeley.edu/Research/Projects/CS/vision/bsds/
[40] Z. Li, X.-M. Wu, and S.-F. Chang, "Segmentation using superpixels: A bipartite graph partitioning approach," in *Proc. IEEE CVPR*, Jun. 2012, pp. 789–796.
[41] C.-Y. Hsu and J.-J. Ding, "Efficient image segmentation algorithm using SLIC superpixels and boundary-focused region merging," in *Proc. 9th Inf., Commun. Signal Process. (ICICS)*, Dec. 2013, pp. 1–5.
[42] K. Parvati, B. S. P. Rao, and M. M. Das, "Image segmentation using gray-scale morphology and marker-controlled watershed transformation," *Discrete Dyn. Nature Soc.*, vol. 2008, Nov. 2008, Art. no. 384346, doi: 10.1155/2008/384346.
[43] D. Comaniciu and P. Meer, "Mean shift: A robust approach toward feature space analysis," *IEEE Trans. Pattern Anal. Mach. Intell.*, vol. 24, no. 5, pp. 603–619, May 2002.
[44] R. Unnikrishnan, C. Pantofaru, and M. Hebert, "Toward objective evaluation of image segmentation algorithms," *IEEE Trans. Pattern Anal. Mach. Intell.*, vol. 29, no. 6, pp. 929–944, Jun. 2007.
[45] M. Meilă, "Comparing clusterings: An axiomatic view," in *Proc. 22nd Int. Conf. Mach. Learn.*, 2005, pp. 577–584.
[46] D. Martin, C. Fowlkes, D. Tal, and J. Malik, "A database of human segmented natural images and its application to evaluating segmentation algorithms and measuring ecological statistics," in *Proc. 8th Int. Conf. Comput. Vis.*, vol. 2. Jul. 2001, pp. 416–423.
[47] J. Freixenet, X. Muñoz, D. Raba, J. Martí, and X. Cufí, "Yet another survey on image segmentation: Region and boundary information integration," in *Proc. 7th Eur. Conf. Comput. Vis.*, Copenhagen, Denmark, May 2002, pp. 408–422.
[48] R. J. Hyndman and Y. Fan, "Sample quantiles in statistical packages," *Amer. Statist.*, vol. 50, no. 4, pp. 361–365, Nov. 1996.
[49] R. K. Falah, P. Bolon, and J. P. Cocquerez, "A region-region and region-edge cooperative approach of image segmentation," in *Proc. ICIP*, vol. 3. Nov. 1994, pp. 470–474.

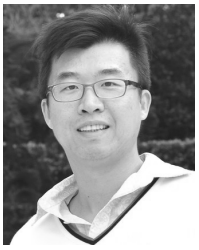

Huang-Chia Shih (M'08) received the B.S. degree (Hons.) in electronics engineering from the National Taipei University of Technology, Taipei, Taiwan, in 2000, and the M.S. and Ph.D. degrees in electrical engineering (EE) from the National Tsing Hua University in 2002 and 2008, respectively.

He served as a Visiting Scholar with the Department of EE, University of Washington from 2006 to 2007. He was a Visiting Professor with the John von Neumann Faculty of Informatics, Obuda University, Hungary in 2011. He has been an Associate Professor with the Department of EE, Yuan Ze University (YZU), Taoyuan, Taiwan, since 2016. He has authored over 50 technical papers in refereed journals and conference proceedings. His research interests are content-based multimedia processing, pattern recognition, and human–computer interaction. He received the Outstanding Youth Electrical Engineer Award from the Chinese Institute of Electrical Engineering in 2015, the YZU Young Scholar Research Award from YZU in 2015, the Kwoh-Ting Li Young Researcher Award from ACM Taipei/Taiwan Chapter in 2014, the Pan Wen Yuan Exploration Research Award from Pan Wen Foundation in May 2013, the best paper awards from IEEE-ISCE 2013, and the IEEE-GCCE 2015.

En-Rui Liu received the B.E. degree from the Department of Computer Science and Information Engineering, Southern Taiwan University of Science and Technology, Tainan, Taiwan, 2006. He is currently pursuing the master's degree with the Department of Electrical Engineering, Yuan Ze University, Taoyuan, Taiwan. His research interests are image morphological processing, image segmentation, and pattern recognition.